agronomy

MDPI

Article

Assessment of the Effects of Newly Fabricated CaO, CuO, ZnO Nanoparticles on Callus Formation Maintenance of *Alfalfa* (*Medicago sativa* L.) Under In Vitro Salt Stress

Mustafa Akçay [1,*], Merve Simsek Geyik [2], Busra Yazicilar [2], Fatma Boke [2], Hayrunnisa Nadaroglu [3,4], Okkes Atıcı [5] and İsmail Bezirganoğlu [2]

[1] Department of Chemistry and Chemical Processing Technologies, Kars Vocational School, Kafkas University, Kars 36000, Türkiye
[2] Department of Molecular Biology and Genetics, Erzurum Technical University, Erzurum 25050, Türkiye; merve98765@gmail.com (M.S.G.); busra.yazicilar21@erzurum.edu.tr (B.Y.); fatmabokee@gmail.com (F.B.); ismail.bezirganoglu@erzurum.edu.tr (İ.B.)
[3] Department of Food Technology, Vocational College of Technical Sciences, Ataturk University, Erzurum 25240, Türkiye; hnisa25@atauni.edu.tr
[4] Department of Nano-Science and Nano-Engineering, Institute of Science, Ataturk University, Erzurum 25240, Türkiye
[5] Department of Biology, Faculty of Science and Arts, Atatürk University, Erzurum 25240, Türkiye; oatici@atauni.edu.tr
* Correspondence: mustafaakcay@kafkas.edu.tr; Tel.: +90-532-169-3687

Abstract: Nanoparticles play an important role in plant response to abiotic stresses including salt stress. In this study, the physiological and histological responses of CuO, ZnO, and CaO nanoparticle (NP) applications on callus tissues developed from two *alfalfa* lines (Erzurum and Muş) exposed to salt (NaCl) stress were evaluated. The NPs were synthesized from the extracts obtained from healthy walnut shells using the green synthesis approach and then characterized by Scanning Electron Microscopy (SEM) and X-ray diffraction analysis (XRD). The leaf explants were placed in an MS medium containing 4 mg L^{-1} 2,4-D (2,4-dichlorophenoxyacetic acid), 50 mM NaCl, and 0.8 ppm of NPs for 1 month in the dark. CaO NP is determined to be more effective than CuO and ZnO in callus induction from leaf explants. Malondialdehyde (MDA) content was higher in the callus treated with 0.8 ppm CuO NP + 50 mM NaCl compared to other treatments. The callus induction stage, without salt treatments, showed the best results with 0.8 ppm CaO NPs for both H_2O_2 levels and peroxidase (POX) activity compared to the other NPs. The highest protein rate was obtained from the callus induction stage and callus formation stage after 50 mM treatment NaCl with 0.8 ppm CuO. The LCSM results displayed, under in vitro conditions, that the treatment of NPs can greatly suppress the negative effects of salt stress on calli samples. SEM analysis supported the results obtained by laser scanning confocal microscopy (LSCM) analysis. Our findings suggest that CuO, CaO, and ZnO NPs can offer a simple and effective method to protect *alfalfa* callus from NaCl stress severity. Furthermore, these NPs, particularly CaO, hold potential for broader application and should be evaluated under various abiotic conditions beyond salt stress.

Keywords: callus; *alfalfa*; nanoparticle; confocal laser scanning analysis; in vitro assay

check for updates

Academic Editor: Essaid Ait Barka

Received: 13 December 2024
Revised: 5 January 2025
Accepted: 10 January 2025
Published: 13 January 2025

Citation: Akçay, M.; Geyik, M.S.; Yazicilar, B.; Boke, F.; Nadaroglu, H.; Atıcı, O.; Bezirganoğlu, İ. Assessment of the Effects of Newly Fabricated CaO, CuO, ZnO Nanoparticles on Callus Formation Maintenance of *Alfalfa* (*Medicago sativa* L.) Under In Vitro Salt Stress. *Agronomy* **2025**, *15*, 180. https://doi.org/10.3390/agronomy15010180

Copyright: © 2025 by the authors. Licensee MDPI, Basel, Switzerland. This article is an open access article distributed under the terms and conditions of the Creative Commons Attribution (CC BY) license (https://creativecommons.org/licenses/by/4.0/).

1. Introduction

Salt stress is becoming an increasingly dangerous environmental issue worldwide [1–3]. Salt-induced damage to crop yield is more severe than other stressors due to the intensity

and duration of the stress. Salt (NaCl) stress decreases root growth, stem expansion, and leaf length, disrupts water use capacity, and lowers plant water activity. Plants exhibit varying metabolic and physiological responses at both the cellular and whole-organism levels in reaction to salt stress, making salt stress a multifaceted challenge. Salt resistance is controlled by numerous physiological strategies, involving complex enzymatic pathways [4–6]. Physiological strategies like osmotic, ionic, and oxidative stress and hormonal imbalances are affected due to salt stress. Salinity adversely affects the growth performance of plants with excess Na^+ and Cl^- ions, which reduce the osmotic potential and prevent nutrient and water uptake in their growth medium [7].

Copper (Cu^{2+}) is an important micronutrient with many functions, including redox reactions participating in the synthesis of chlorophyll and the metabolism of carbohydrates and protein. The tolerance of diseases and crop yields can be influenced by a deficiency in Cu^{2+} [8]. Zinc (Zn^{2+}), as an essential micronutrient, participates directly in plant metabolic activities such as the formation of protein and carbohydrates, the synthesis of chlorophyll, and the synthesis of auxins from tryptophan [9]. Plants deficient in Zn^{2+} experience reduced crop productivity and lower quality in the harvested crops [10]. Calcium (Ca^{2+}) is also an essential element needed for the growth and development of plants. It performs a dual function, as it is not only a crucial microelement for cell wall stability but also plays a role as a secondary messenger in many biochemical and physiologic processes of plants in response to environmental stresses [11]. The advantages of nanoparticles are their availability in lower quantities and the ability of plants to benefit more easily. CaO NP ameliorated the excessive injury effect of salinity by upregulating the performance of the plants [12]. CuO/ZnO stands out for its ability to alleviate salt stress in plant species and promote plant growth under stress environments [13].

Nanotechnology has a larger application than biotechnology, containing gene transformation, genomics, proteomics and bioinformatics, and other technologies [14,15]. Within this approach, nanoparticles have assisted crop productivity development by introducing qualities such as biotic resistance and increased abiotic stress resistance. The green nanoparticles derived from plants are more economical and eco-friendly [16,17]. Studies have reported that exogenous applications of certain nanoparticles have both favorable and unfavorable effects on plant growth and development processes, depending on the applied concentration, application strategy, and plant species studied [15,18,19]. For instance, CuO and ZnO oxide nanoparticles can protect plants against stress factors by improving the activity of cytosolic enzymes [20]. Also, CaO NP synthesized from certain marine molluscan shells at a concentration of 250 ppm promoted seed germination, radicle growth, seedling length, and vigor index in mung beans (*Vigna radata*) [21]. In addition, our last study found that CaO nanoparticles improved some biochemical and physiological parameters associated with salt stress in triticale callus exposed to short- and long-term salt stress [22]. However, the physiological and molecular responses of callus cells to NPs are still unclear [6,23].

Plant tissue culture could serve as an important means to improve crop tolerance in response to salt stress and it has great advantages compared to conventional whole-plant cultivation, which includes limited space and time. In vitro, the selection of salt-resistant lines and regenerated plants has been reported in several plant species. Therefore, the in vitro culture method suggested appears to be a good tool for studying the physiological and biochemical processes involved in plant cultivars' response to salt stress [24]. Callus culture is a suitable resource for rapidly producing high-quality shoots and bio-active phytochemicals. Callus can be stimulated further for the in vitro propagation of whole plants and used to deliver NPs into plants. The treatments of NPs in callus culture increased their content of bioactive molecules in response to biotic and abiotic stress factors [6,20].

Developing innovative strategies to characterize and clarify the interaction of nanoparticles with plant cells and tissues would provide a better understanding of their potential effects in in vitro plant culture. To date, microscopy techniques have been used to study the assimilation and accumulation of NPs in plants under in vitro conditions.

Alfalfa (*Medicago sativa* L.) is used in livestock feed and is superior to other forage crops in terms of nutritional quality [25]. Planted intensively almost all over the world, *alfalfa* has rich nutritional value as the source of proteins, carbohydrates, vitamins, minerals, and dietary fibers; additionally, it contributes to the enrichment of the nitrogen content of agricultural soils [26]. However, *alfalfa* production is severely reduced by salt stress.

Understanding the response of *alfalfa* plants toward salinity stress at the nano-based level and developing salt-resistant cultivars are vital mandates for its effective management. To our knowledge, no previous research article has shown the effects of CuO, CaO, and ZnO NPs on callus biomass formation and the production of antioxidants in callus cultures of *alfalfa*. Therefore, the overall objective of the current study was to evaluate the possible effects of NPs on callus induction, biomass formation, and extension of desirable levels of resistance to salt stress in *alfalfa*. For this aim, the levels of H_2O_2 and lipid peroxidation (as malondialdehyde content), peroxidase (POX) activity, and histological tissue examination were determined in the callus cultures under salt stress exposure using Scanning Electron Microscopy and a laser scanning confocal microscope (CLSM) (Figure 1).

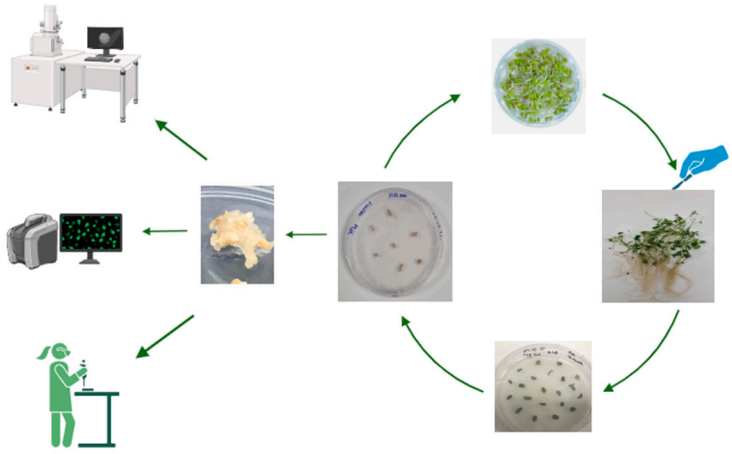


Figure 1. Callus induction and methodology.

2. Materials and Methods

2.1. Plant Material and Callus Induction

In our study, two *alfalfa* lines (Erzurum and Muş) were used as the material for the response to CaO, CuO, and ZnO NPs. The mature seeds were sterilized with 1% NaOCl for 5 min, washed several times with sterile distilled water, and rinsed by changing sterile distilled water overnight at 4 °C. The mature seeds were cultivated in Petri dishes containing full MS medium [27] for 30 days at 25 ± 1 °C and in 16/8 h light/dark photoperiods at 650 µmol m^{-2} s^{-1} illumination intensity. Leaves were removed aseptically using forceps, placed on the MS medium [27], containing 2 mg L^{-1} glycine, 4 mg L^{-1} 2,4-D (2,4-dichloro phenoxy acetic acid), 100 mg L^{-1} Myo-inositol, 0.5 mg L^{-1} nicotinic acid, 0.5 mg L^{-1} pyridoxine HCl, 0.1 mg L^{-1} thiamine HCl, 1.95 g MES, 50 mg L^{-1} ascorbic acid, 20 g sucrose, and solidified with 7 g of agar; then, the pH was adjusted to 5.8 before autoclaving. In the sterilization of the vitamins and hormones, 0.22 µm of porous cellulose nitrate filters were used and 0.8 ppm CaO, CuO, and ZnO NPs were added. The leaves were incubated in total darkness at 25 ± 1 °C for one month.

2.2. Green Synthesis and Structural Characterization of the NPs

CuO, CaO, and ZnO NPs were synthesized from the walnut shell extract using the green synthesis method previously used by Nadaroglu et al. 2017 [28]. For this, the walnut shells to be used in the green synthesizing of CaO, CuO, and ZnO NPs were collected from the walnut gardens in Erzurum (Turkey) in August–September 2020 and kept in the refrigerator at +4 °C until they were studied. Walnut shells (25 g) were first washed with distilled water and then the walnut shells were broken. The solid particles were then separated from the solution by filtration using filter paper (Watman 1). CaO, CuO, and ZnO NPs were synthesized using obtained walnut shell extract and 0.1 M $Ca(NO_3)_2$, $Zn(NO_3)_2$, and $Cu(NO_3)_2$ solutions [28].

2.3. Characterization of CaO, CuO, and ZnO NPs

The characterization of CaO, CuO, and ZnO NPs was carried out at the Eastern Anatolia High Technology Application and Research Center (DAYTAM) affiliated with Atatürk University, Erzurum (Turkey). Scanning Electron Microscopy (SEM) and X-ray diffraction (XRD) analysis were used for the characterization of CaO, CuO, and ZnO NPs. In this way, information about the size and morphological properties of synthesized nanoparticles was obtained.

2.4. Salt Stress Treatment and NPs Applications

Erzurum and Muş leaf explants were used for callus formation in MS [27] medium containing 4 mg L^{-1} 2,4-D and 0.125 mg kinetin, including 0.8 ppm CaO, CuO, and ZnO NPs. The total culture duration was one month. Then, callus was obtained from 50 mM NaCl, with exposure times of one week and two weeks. Callus was transferred to hormone MS medium [27], containing 1.0 mg L^{-1} 2,4-D and 1 mg L^{-1} kinetin in the presence of 50 mM NaCl, including 0.8 ppm CaO, CuO, and ZnO NPs.

2.5. Determination of Lipid Peroxidation Level

Lipid peroxidation level (LPO) is determined by measuring malondialdehyde (MDA) content [29]. Callus tissue (0.4 g) was homogenized using liquid nitrogen and then dispersed in 20% (*w*/*v*) trichloroacetic acid (TCA) containing 0.5% (*w*/*v*) thiobarbituric acid (TBA) solution. The sample was boiled at 98 °C for 30 min and then quickly taken into an ice bath. The sample content was centrifuged at 3000× *g* for 10 min, and the value of the supernatant was monitored at 532 and 600 nm [29,30].

2.6. Determination of Hydrogen Peroxide Content

Hydrogen peroxide (H_2O_2) content was measured using the method of Velikova et al. (2000) [31]. Callus material (0.4 g) was homogenized in 4 mL of trichloroacetic acid and centrifuged at 4 °C for 15 min at 13,000 rpm. An amount of 2 mL of extract was mixed with 0.8 mL of KH_2PO_4 and 1.6 mL of KI in test tubes. The absorbance of the callus sample product was measured at 390 nm using a standard curve with H_2O_2 solutions.

2.7. Determination of Peroxidase Activity

Guaiacol peroxidase (POX) activity was measured following the procedure established by Yee et al. (2003) [32] by adding 100 µL of the callus extract to 3 mL of assay solution, which contained 13 mM guaiacol, 5 mM H_2O_2, and 50 mM Na-P buffer (pH 6.5). POX activity was determined in absorbance at 470 nm of protein. The total soluble protein contents were determined by the BCA (Bicinchoninic Acid) protocol.

2.8. Sectioning with Microtonal

Having been kept in 10% formaldehyde for 3 days, callus structures were taken to the cassettes and left for an overnight wash. Then, it was kept in 70, 80, and 96% ethyl alcohol, one hour apart, respectively. Absol-I, Absol-II, Xylol-I, and Xylol-II were kept for 1 h, respectively. The calluses were embedded in parafilm, and a section of 6 µm was taken [33].

2.9. Laser Scanning Confocal Microscope (CLSM)

Callus, sectioned with microton, was kept for about 30 min with 1% rhodamine. Then, it was passed through distilled water 3 times. Fluorescence images were obtained with a Zeiss LSM 710 Confocal Laser Scanning Microscope (Oberkochen, Germany). Samples were excited with the 488 nm line of an argon laser and dye emission was collected at 520 and 610 nm. The DCF fluorescence was visualized in a single optical section of the callus. All images were obtained at the same depth [34].

2.10. Scanning Electron Microscopy

Alfalfa callus tissues were prefixed in 5% buffered glutaraldehyde (0.1 M phosphate buffer, pH 7.2) for 2 h at room temperature. After dehydration through a graded ethanol series, samples were dried with a CPD (CO_2 critical-point drying) system, sputter-coated with gold (Jeol JFC-1100 E ion-sputtering system, Ibaraki, Japan), and observed with a scanning electron microscope (HITACHI S-4700, Ibaraki, Japan).

2.11. Statistical Analysis

Each experiment was repeated three times. Analysis of variance was conducted using a one-way ANOVA test using SPSS 13.0 and means were compared by Duncan's test at the 0.05 confidence level.

3. Results

3.1. Result of Analysis of CaO, CuO, and ZnO NPs

The surface morphology examination of synthesized CaO, CuO, and ZnO NPs was carried out using a Zeiss brand Sigma 300 model scanning electron microscope (SEM, 8010 Graz Austria). Figure 2 shows that CaO NPs have a particle size ranging from 35 to 160 nm. According to SEM images, CaO NPs are porous, and the structure is regular and has a very pleasant layered structure (Figure 2A). The SEM analysis revealed that CaO NPs have a particle size range of 35 to 160 nm (Figure 2A). The SEM images further indicate that CaO NPs exhibit a porous, layered structure with regular morphology. These findings are consistent with the results reported by Anantharaman and George and Meshkatalsadat et al., which support the green synthesis approach. It is clearly understood from the SEM images that the CaO NPs obtained by the green synthesis method have a layered structure due to their properties and a single dimension at 35–160 nm as stated in the article. In another dimension, it is seen that they are stacked on top of each other in a layered structure. In the study, CaO NPs were applied to *alfalfa* plants in completely dissolved form, not in solid form. The SEM findings obtained by Anantharaman and George and Meshkatalsadat et al. as a result of green synthesis of CaO NPs support our study [35,36]. Similarly, ZnO NPs were found to have particle sizes ranging from 17 to 65 nm, with a rough and agglomerated spherical structure, as shown in Figure 2B. These findings align with the XRD results, confirming the crystalline and structural features of ZnO NPs. For CuO NPs, the SEM images indicate spherical shapes with sizes distributed between 20 and 45 nm (Figure 2C). The spherical morphology and size distribution are consistent with the literature and supported by XRD analysis.

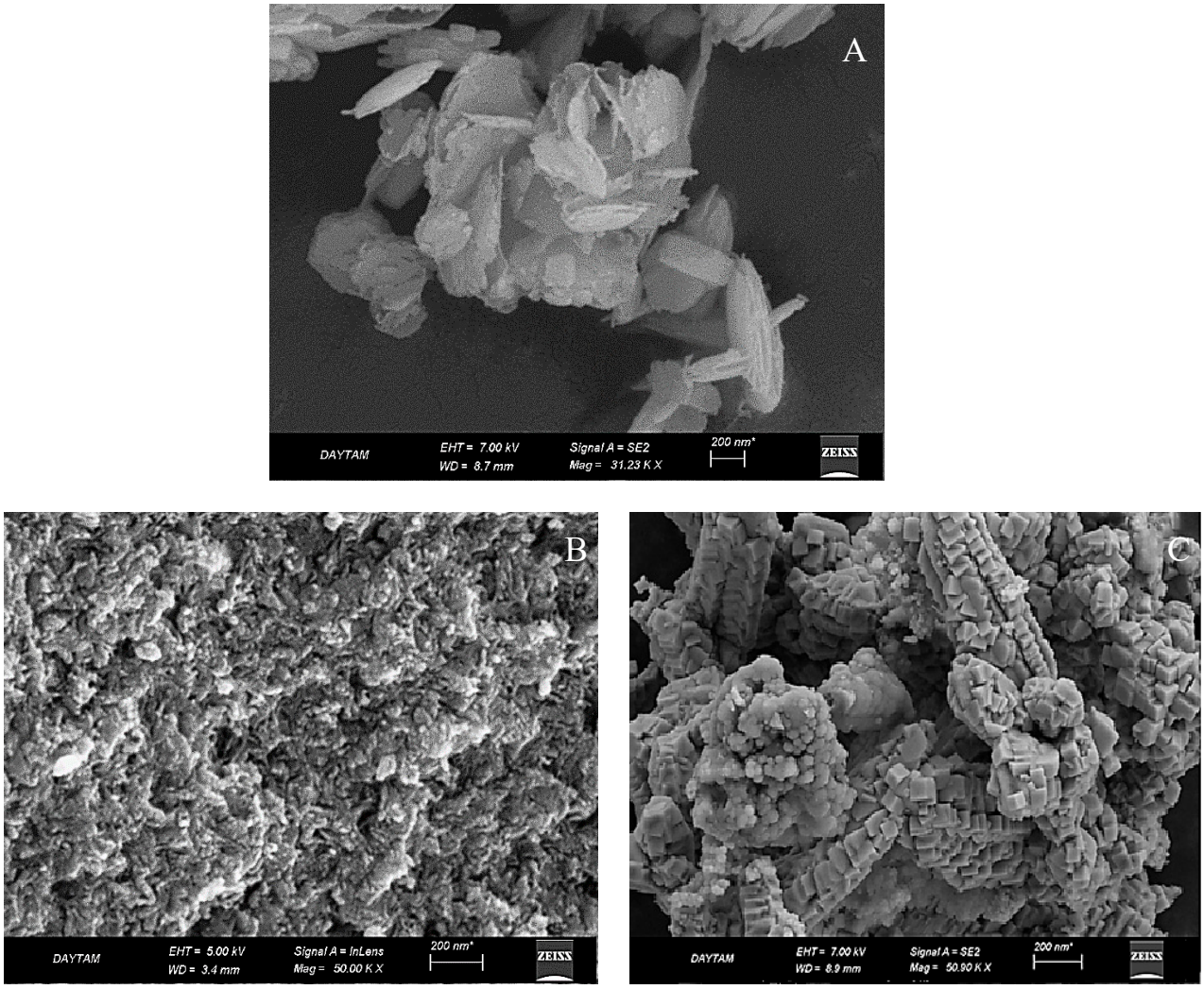


Figure 2. SEM images of CaO NPs (**A**), ZnO NPs (**B**), and CuO NPs (**C**).

Furthermore, the crystallite sizes of the nanoparticles were calculated using the Scherrer equation:

$$D = \frac{k\lambda}{\beta cos\theta} \times 100$$

where

D is the crystallite size;

k is the shape factor (typically 0.9 for spherical particles);

λ is the X-ray wavelength (1.5406 Å for Cu Kα radiation);

β is the full width at half maximum (FWHM) of the diffraction peak in radians;

θ is the Bragg angle.

For CaO NPs, the calculated crystallite sizes were consistent with the SEM results, confirming the size range of 35–160 nm. Similarly, ZnO and CuO NPs showed crystallite sizes of 17–65 nm and 20–45 nm, respectively, aligning with the dimensions observed in SEM images.

The combination of SEM analysis and XRD-based crystallite size calculations using the Scherrer equation verifies that the synthesized nanoparticles fall within the nanoregulator range. These details have been incorporated into the revised manuscript to address the reviewer's comment comprehensively.

3.2. X-Ray Diffraction Analysis

The spectra of the XRD analysis (X-ray diffraction) of the CaO NPs structure are shown in Figure 3. The peaks at 28.75°, 34.16° (111), 47.11°, 50.86° (311), 54.60° (222), and 62.60° indicate Ca^{2+}, carbohydrate units, and CaO NPs [22,37]. The findings obtained confirmed that the structure of CaO NPs was successfully formed. Zn NPs structures were determined to be cubic (fcc) zinc nanocrystals [38]. XRD and crystallographic analysis of CuO nanoparticles synthesized by the green synthesis method are given in (Figure 3B); 2 θ = 32.2°, 39.62°, 58.9°, and 70.3° of the XRD spectrum showed characteristic peaks that can be indexed at facets (110), (111), and (202) (Figure 3B). It has been determined that CuO NPs structures have a spherical structure [39]. XRD and crystallographic analysis of CuO nanoparticles by green synthesis method using walnut shell extract are given in (Figure 3C). The characteristic peaks of the XRD spectrum that can be indexed at 2 fas = 11.39°, 22.24°, 36.09°, 49.22° and facets (111), (200), (220) are consistent with the literature.

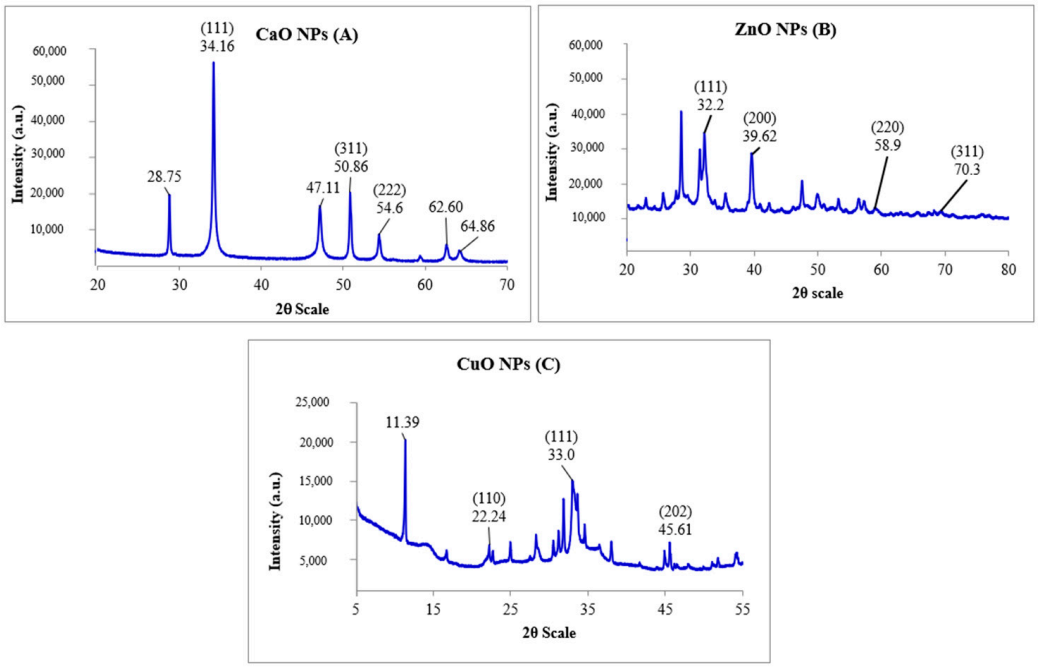


Figure 3. XRD patterns CaO NPs (**A**), ZnO NPs (**B**), CuO NPs (**C**).

3.3. Lipid Peroxidation Level (As MDA)

The callus induction stages of the Erzurum (resistant line) and Muş (sensitive line) genotypes produced as a result of ZnO, CuO, and CaO NP application against NaCl were evaluated. Also, salt-free ZnO, CuO, and CaO NPs applied to callus formation stages were evaluated. MDA content was greatly affected in the callus formation stage of two *alfalfa* lines in the presence of 0.8 ppm NPs after salt treatments (Table 1). MDA values indicated a large range of variation among tested samples for salt stress treatments, ranging from 0.0168 to 0.0466 nmol g^{-1} FW. The maximum content was observed from the callus treated with 50 mM NaCl + 0.8 ppm CuO NPs. The callus induction stage without salt treatments indicated the best result in 0.8 ppm CaO NPs for MDA value compared to the other NPs. Although the highest LPO was found in the treatments with 0.8 ppm CuO 50 mM NaCl in the callus induction stage, the lowest LPO was found in the 'callus formation stage' for 0.8 ppm CaO NPs 50 mM NaCl (Table 1).

Table 1. Effect of the NPs on the contents of MDA, H_2O_2, soluble protein, and POX activity in the callus tissues.

Treatments	MDA (ng g^{-1} FW)	POX Activity (EU mg^{-1} Protein)	Soluble Protein (mg g^{-1} FW)	H_2O_2 (ng g^{-1} FW)
0.8 ppm ZnO (+)	0.0210 ± 0.005 ^{e}	1.4727 ± 0.186 ^{ab}	2.0439 ± 0.260 ^{a}	0.0386 ± 0.014 ^{bc}
0.8 ppm CuO (+)	0.0411 ± 0.005 ^{bc}	1.2792 ± 0.186 ^{ab}	1.5331 ± 0.260 ^{a}	0.0979 ± 0.014 ^{a}
0.8 ppm CaO (+)	0.0194 ± 0.005 ^{e}	0.9267 ± 0.186 ^{b}	1.7457 ± 0.260 ^{a}	0.0319 ± 0.014 ^{bc}
0.8 ppm ZnO 50 mM NaCI (+)	0.0329 ± 0.005 ^{bcde}	1.1658 ± 0.186 ^{ab}	2.0548 ± 0.260 ^{a}	0.0481 ± 0.014 ^{bc}
0.8 ppm CuO 50 mM NaCI (+)	0.0466 ± 0.005 ^{b}	1.5335 ± 0.186 ^{ab}	2.4061 ± 0.260 ^{a}	0.0377 ± 0.014 ^{bc}
0.8 ppm CaO 50 mM NaCI (+)	0.0831 ± 0.005 ^{a}	1.2862 ± 0.186 ^{ab}	2.4005 ± 0.260 ^{a}	0.0645 ± 0.014 ^{ab}
Control	0.0410 ± 0.005 ^{bc}	0.9985 ± 0.186 ^{b}	1.1589 ± 0.260 ^{a}	0.0545 ± 0.014 ^{bc}
50 Mm NaCI	0.0250 ± 0.005 ^{cde}	1.6668 ± 0.186 ^{a}	1.7398 ± 0.260 ^{a}	0.0388 ± 0.014 ^{bc}
0.8 ppm ZnO (−)	0.0236 ± 0.005 ^{de}	0.9699 ± 0.186 ^{b}	1.9880 ± 0.260 ^{a}	0.0293 ± 0.014 ^{bc}
0.8 ppm CuO (−)	0.0323 ± 0.005 ^{bcde}	0.1035 ± 0.186 ^{c}	0.6741 ± 0.260 ^{b}	0.0134 ± 0.014 ^{c}
0.8 ppm CaO (−)	0.0445 ± 0.005 ^{b}	1.0015 ± 0.186 ^{b}	1.6147 ± 0.260 ^{a}	0.0389 ± 0.014 ^{bc}
0.8 ppm ZnO 50 mM NaCI (−)	0.0312 ± 0.005 ^{bcde}	0.9742 ± 0.186 ^{b}	1.6574 ± 0.260 ^{a}	0.0289 ± 0.014 ^{bc}
0.8 ppm CuO 50 mM NaCI (−)	0.0384 ± 0.005 ^{bcd}	1.0663 ± 0.186 ^{ab}	2.3167 ± 0.260 ^{a}	0.0450 ± 0.014 ^{bc}
0.8 ppm CaO 50 mM NaCI (−)	0.0168 ± 0.005 ^{d}	1.4176 ± 0.186 ^{ab}	1.9674 ± 0.260 ^{a}	0.0445 ± 0.014 ^{bc}

Different letters in the same column refer to significant differences at the $p \leq 0.05$ significance level. ± means SE. FW: Fresh weight.

3.4. H_2O_2 Content

There were significant differences among 1. week Muş callus and the other groups (Figure 3). Figure 3 shows the characterization of nanoparticles and not the differences between groups of experiments. Table 1 displays that H_2O_2 levels were significantly affected in the tested callus of two *alfalfa* lines in the presence of 0.8 ppm NPs. H_2O_2 values indicated a large range of variation among tested samples for salt stress treatments, ranging from 0.0134 to 0.0979 nmol g^{-1} FW. The callus induction stage without salt treatments indicated the best result in 0.8 ppm CaO NPs for the H_2O_2 value compared to the other NPs. Although the highest H_2O_2 value was found in the treatments of 0.8 ppm CuO NPs in the callus induction stage, the lowest H_2O_2 value was found in the callus formation stage for 0.8 ppm CuO NPs (Table 1).

3.5. POX Activity

POX activities were significantly affected in the callus formation stage of two *alfalfa* lines in the presence of 0.8 ppm NPs (Table 1). POX values indicated a large range of variation among tested samples for salt stress treatments, ranging from 0.1035 to 1.666 nmol g^{-1} FW. The maximum activity was observed from the callus treated with 50 mM NaCl. The callus induction stage without salt treatments indicated the best result in 0.8 ppm CaO NPs for POX activity compared to the other NPs. Although the highest activity was found in the treatments of 50 mM NaCl, the lowest activity was found in the 'callus induction stage' for 0.8 ppm CuO NPs (Table 1).

3.6. Soluble Protein Content

The results indicated that protein levels were more significantly affected in the Muş and Erzurum callus (Figure 4). However, only minimal protein accumulation was detected in the control callus, except at 0.8 ppm CuO. CuO resulted in lower protein accumulation compared to NaCl treatment. The highest response was observed during the callus induction and formation stages following a 50 mM NaCl treatment with 0.8 ppm CuO. In contrast, the best response without NaCl was seen in the callus induction and formation stages with 0.8 ppm ZnO (Table 1).

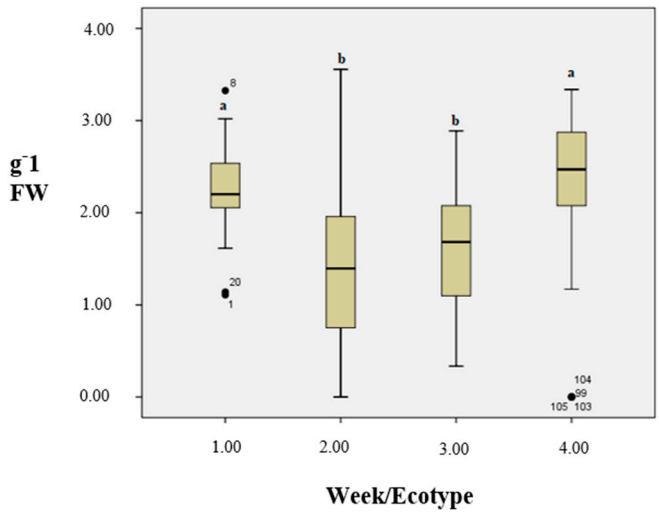


Figure 4. Changes in protein content *alfalfa* genotypes: 1: First week Muş, 2: First week Erzurum, 3: Second week Muş, 4: Second week Erzurum 1: First week Muş, 2: First Erzurum, 3: Second week Muş, 4: Second week Erzurum. [a,b] Values with different superscript letters in the same column indicate significant differences ($p \leq 0.05$).

3.7. Laser Scanning Confocal Microscope (LSCM)

LSCM was used as a visual marker to verify the distribution of nanoparticles in a stable callus culture. NaCl-free callus and callus treated with 50 mM NaCl alone were used as a control. The analysis showed that the CaO, CuO, and ZnO NPs are traceable in the Erzurum and Muş callus tissues (Figure 5). However, the NaCl stress inhibited in terms of nanoparticles was at different degrees. CuO exhibited a better response than CaO and ZnO NPs in response to NaCl stress. In the first week, the accumulation of NPs inside the cell had lower activity with NaCl than in the second week in terms of Erzurum and Muş genotypes. According to the results of the confocal analysis, CuO exhibited the most abundant callus induction stage, followed by ZnO exhibited at the callus induction stage, 50 mM NaCl and ZnO callus induction stage, and, finally, 50 mM NaCl CuO callus induction stage (Figure 5).

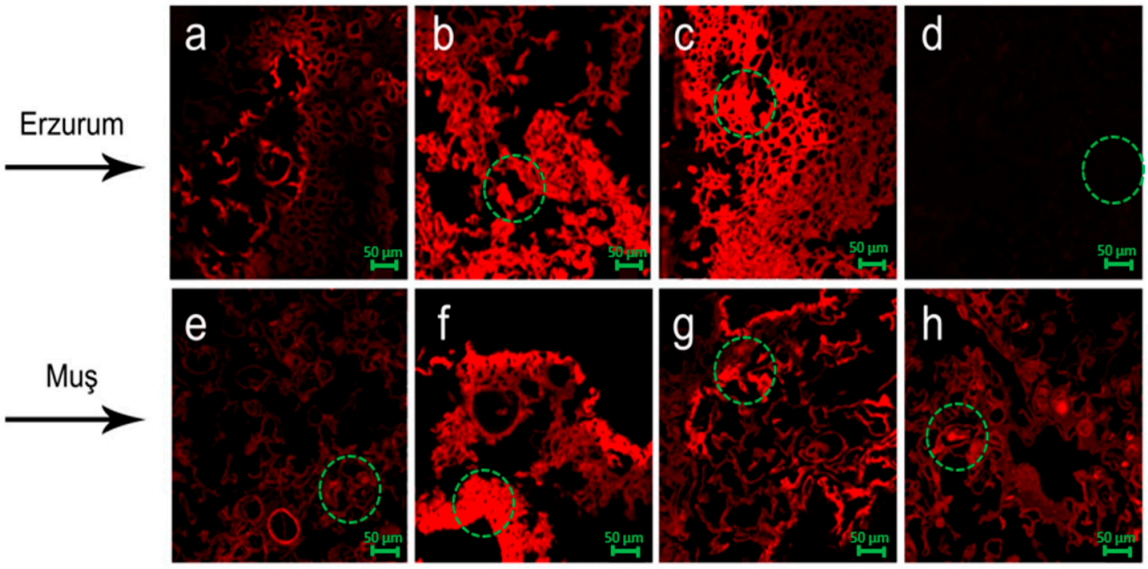


Figure 5. Image of confocal microscope: (**a**) Erzurum control, (**b**) Erzurum 50 mM NaCl, (**c**) Erzurum 0.8 ppm CuO (+), (**d**) Erzurum 0.8 ppm CaO 50 mM NaCl (−), (**e**) Muş control, (**f**) Muş 50 mM NaCl, (**g**) Muş 0.8 ppm ZnO (+), (**h**) 0.8 ppm CaO 50 mM NaCl.

3.8. SEM Analysis of Callus Structures

SEM detection indicated that each genotype callus type had various callus structures. There was a continuous amorphous sphere, termed extracellular matrix, on the callus surface. It was also detected that cultivars belonging to the same genotypes share similar cell structures and shapes. The soft and compact character of the callus in Erzurum and Muş converted to a granular, mucilage-like structure, mostly like a membranous surface and wrinkled cell mass structure under SEM detections (Figure 6).

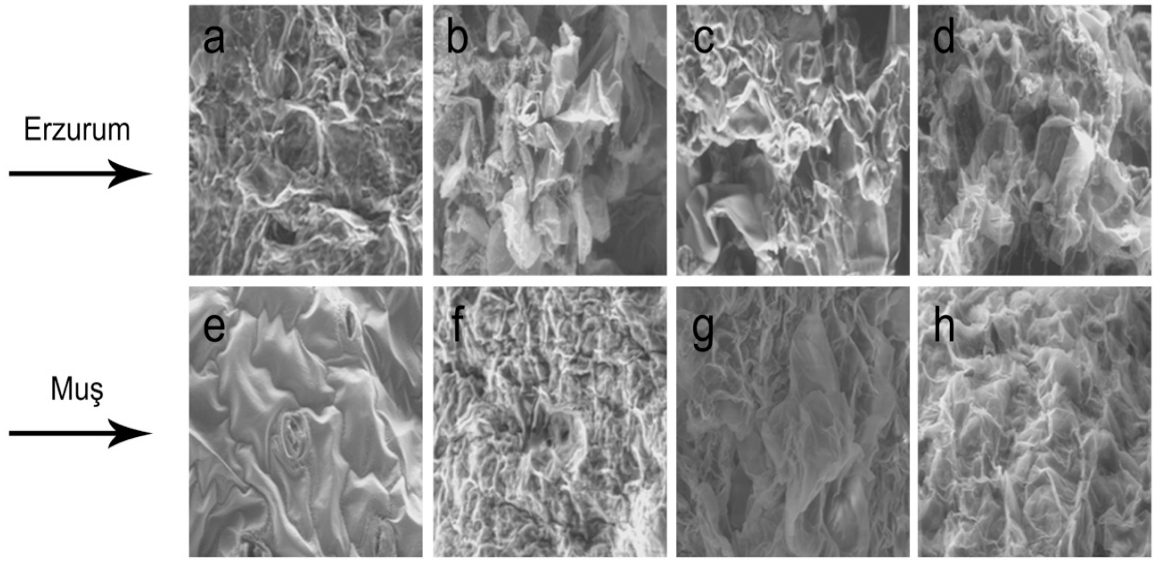


Figure 6. İmage of SEM: (**a**) Erzurum control, (**b**) Erzurum 50 mM NaCl, (**c**) Erzurum 0.8 ppm CuO (+), (**d**) Erzurum 0.8 ppm CaO 50 mM NaCl (−), (**e**) Muş control, (**f**) Muş 50 mM NaCl, (**g**) Muş 0.8 ppm ZnO (+), (**h**) Muş 0.8 ppm CaO 50 mM NaCl.

4. Discussion

Many studies reported that using nanoparticles could regulate plant species' response mechanisms to stress factors. In particular, recent studies highlighted the effects of nanoparticles on plants under in vitro tissue culture conditions, including the molecular mechanisms underlying stress responses in the presence of nanoparticles [40,41]. These findings emphasize the role of nanoparticles in modifying cellular responses and mediating stress tolerance in plant tissues. This study investigated the effects of CaO, CuO, and ZnO nanoparticle applications on callus induction responses in calli from two *alfalfa* lines developed under salt stress conditions by evaluating certain physiological and histological parameters. It displayed significant differences in their responses to the NPs. Callus induction in the presence of NPs was found to occur more rapidly compared to the control group, consistent with findings that nanoparticles enhance cellular metabolic activity under in vitro conditions [42]. The results showed that NPs promoted callus induction, whereas control callus showed a delayed initiation of induction compared to NPs treatments. The obtained results show that compact callus with a globular structure and a yellowish color callus were formed from leaf explants within 1 month, while there was callus induction in the NPs within a shorter time of 1 month. Callus induction occurred at varying frequencies depending on the NP treatments. The highest frequency of callus induction from leaf explants of Muş genotype was detected on the medium containing 0.8 ppm CaO. Notably, the effects of CaO nanoparticles may be attributed to their ability to rapidly accumulate within the callus tissues and trigger signaling cascades associated with stress response mechanisms [42]. Among tested treatments, CaO is evident to be more effective than CuO and ZnO in callus induction from leaf explants. The fresh weight in Muş callus in the presence of 0.8 ppm CaO was heavier than those of CuO and ZnO in equal concentration. Noticeably, the size of all tested NPs examined in this study was identical, with a value of 20–160 nm, but varying uptake and accumulation functions of those three types of NPs were detected, and the genotype-dependent uptake for NPs occurred in the callus. This observation aligns with recent studies reporting that nanoparticle size and surface chemistry influence their uptake and bioavailability in plant tissues under stress conditions [40]. Previous studies have shown a positive correlation between NaCl and nanoparticle accumulation in various plant species [43,44]. For example, Shoukat et al. [45] demonstrated the

intricate roles of nanoparticles in mediating stress responses and cellular alterations under abiotic stress conditions in plants. Ca^{2+} ions are rapidly carried by membrane channels that are available on the plasma surface [46,47]. This confirms that CaO in the culture medium was quickly responsive and effectively accumulated. In terms of confocal analysis, the assessment of NPs functions in the presence of NaCl was based on the expanded coloration, tissue damage, and amount of cell survival. In our cases, the results of laser scanning confocal analysis and SEM demonstrated that the delivery of NPs in *alfalfa* callus is related to the uptake of nutrient elements and translocated from the culture medium (Figure 5). CuO nanoparticle application in the Muş genotype in the 1st week provided an expected improvement in NaCl stress. CuO application showed a dense distribution in the cell by preventing the adverse effect of 50 mM salt faster than ZnO and CaO applications. The best response of ZnO nanoparticle application was obtained in the 2nd week of the Muş genotype compared with the 1st week and the 2nd week. ZnO accumulated intensely in certain parts of the cell in 1st week of application, and, as the period extended, it simultaneously distributed into the cell and prevented the negative effect of salt. These indicate that term alterations of defense responses to NaCl could be a main process. One or two weeks post-NaCl application, the control callus displayed salt severity on the callus tissues, resulting in tissue damage within less than 7 days (Figure 5). In contrast, Muş and Erzurum genotypes with the first application of CuO NPs survived longer than 2 weeks, indicating considerably improved resistance to NaCl. Our detection of NPs in callus tissues following a fairly aggressive second application suggests that CaO, CuO, and ZnO were present, not merely on the extracellular matrix, but that it penetrated inside the callus cells. SEM analysis supported the confocal analysis results, indicating that CuO disrupted the *alfalfa* callus's extracellular matrix 7 days post-exposure (Figure 5c). Fourteen days post-exposure, CuO was located inside callus cell tissues. In alignment with these findings, Al-Khayri et al. (2023) [48] reported that nanoparticle penetration and their interaction with intracellular structures enhance stress tolerance in plant tissues.

It was detected that the formation of the alfalfa callus structure subject to media including various NPs such as CaO, CuO, and ZnO can be added to the culture media. It was noticed that there was no harm to the cell wall in the callus of the control while harm was detected in the cell wall of the callus exposed to 50 mM NaCl (Figure 6). This is evident that even lower doses of NaCl dramatically increased the damage to the cell walls of the callus tissues. Callus produces an amorphous mass of extreme cell walls in response to exposure to different time periods (Figure 6). The accumulation of NPs and their adverse effects on applied callus tissues highly depend on the genotype and exposure time. It has also been recently shown that nanoparticle effects depend significantly on their surface properties and interaction with the plant extracellular matrix [48]. In our study, 7 days post-exposure, ZnO NPs exhibited membranous structures associated with the extracellular matrix and neighboring cells, and they were rich in ZnO, which accumulated and was present in the 50 mM NaCl. In contrast, CuO NPs showed partial roughness and mucilage-like structures on the fibroblast in Erzurum genotypes. The CaO NPs exhibited wrinkles and rough structures in the 1st week of the Erzurum genotype. In the 1st week of the application of 50 mM NaCl of the Muş genotype, mostly granular structures and nodular callus segments were shown. In the 2nd week, the Muş genotype exhibited mucilage-like structures and the differentiation of the callus primordia, while the Erzurum genotype displayed wrinkle-like structures when exposed to 50 mM NaCl (Figure 6). Callus exposed to NaCl during the 2nd week demonstrated better physiological properties, irrespective of the nanoparticle type, suggesting improved regeneration capacity. This supports the notion that the chemical composition and structural regulation of callus tissues are crucial for morphological development. Medium conditions in tissue culture induced the activation

of various cellular defense strategies, adjusting cell adaptation under new environmental conditions. These findings are consistent with one of the first reports on the formation of the ECM mediated on the outer surface layer [49]. Al-Khayri et al. [48] also emphasized similar observations, showing that nanoparticle-mediated physiological alterations promote plant adaptability to stressful conditions. They suggested that ECM formation might be a stress response of explants, revealed by specific tissue culture conditions.

As outlined by Al-Khayri et al. (2023) [48], MDA and other oxidative stress markers provide insights into the tolerance mechanisms modulated by nanoparticles under abiotic stresses. In our study, NaCl severity resulted in an obvious increase in MDA values in the callus. A reduction in MDA content was also observed in the callus formation stage subject to 0.8 ppm CaO 50 mM NaCl. Based on genotype, the NPs applied to the callus had considerably higher MDA values compared with the 1st and 2nd weeks. This indicated that NaCl-activated stress severity was alleviated by ZnO, CuO, and CaO (Figure 7), and the effect of NPs was linked to the callus structure and genotypes. These findings are in agreement with one of the reports on the absence of NP-mediated tolerance to NaCl stress in potato calli [50]. The levels of MDA in callus induction stages were higher than the callus formation stage in callus cells of both genotypes. The obtained results suggested that MDA content from the callus induction stage was higher, promoting NPs uptake and binding capacity in the cytosol even without NaCl. This verifies that the NaCl-induced stress was mitigated by nano-CaO, -CuO, and -ZnO.

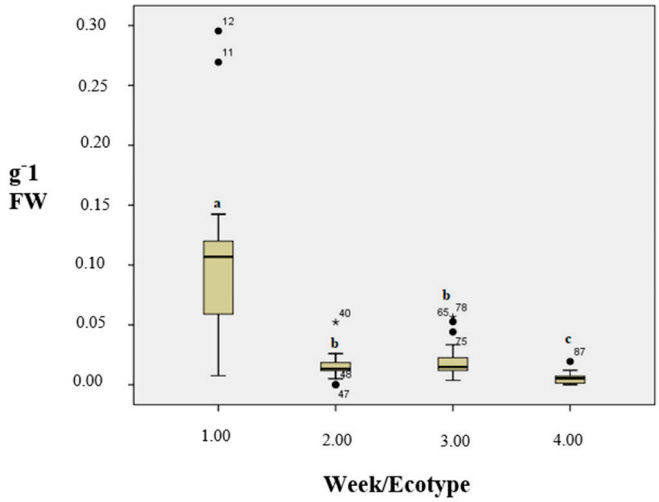


Figure 7. Changes in MDA content *alfalfa* genotypes: 1: First week Muş, 2: First week Erzurum, 3: Second week Muş, 4: Second week Erzurum. [a,b,c] Values with different superscript letters in the same column indicate significant differences ($p \leq 0.05$). * Significantly different at $p = 0.05$.

Nano-induced ROS balance and H_2O_2 modulation might also be linked to augmented antioxidant activity ,as suggested in other relevant studies [45]. Under stress conditions, H_2O_2 is generated and mediates crosstalk among metabolic processes. Therefore, H_2O_2 is a signaling molecule that participates in the events [51]. In our cases, the results verified that the production of H_2O_2 is dependent on genotype and nanoparticle types. However, the application of the Muş genotype and the Erzurum genotype in the 1st week was significantly different from the 2nd week, and there was higher H_2O_2 production at the callus formation stage in the presence of CuO NPs. Additionally, the application of long-period callus cells with CuO considerably recovered stress severity at the callus formation stage (Figure 8). These results are attributed to the outcomes obtained on callus cell tissues in different Triticale genotypes [22]. The POX activity with callus tissues with NPs was considerably decreased when exposed to the control in the presence of 50 mM NaCl.

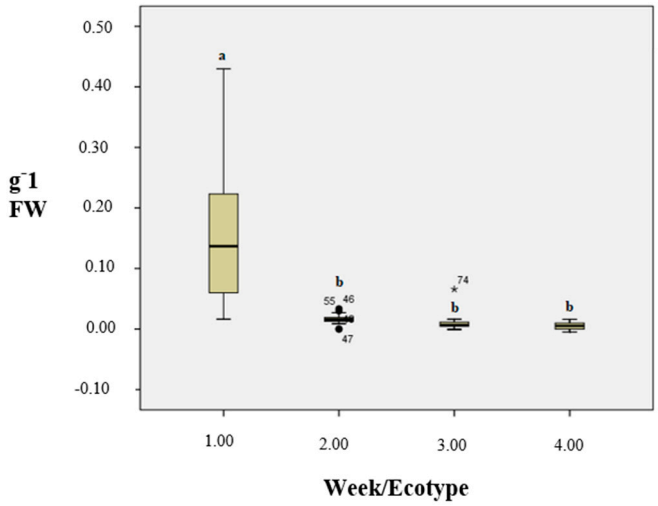


Figure 8. Changes in H_2O_2 content *alfalfa* genotypes: 1: First week Muş, 2: First week Erzurum, 3: Second week Muş, 4: Second week Erzurum 1: First week Muş, 2: First Erzurum, 3: Second week Muş, 4: Second week Erzurum. [a,b] Values with different superscript letters in the same column indicate significant differences ($p \leq 0.05$). * Significantly different at $p = 0.05$.

Molecular studies revealed that the presence of nanoparticles in tissue culture media can regulate antioxidant enzyme activities and other stress-associated pathways, thereby enhancing callus development and viability [41]. This molecular insight can provide a better understanding of the distinct effects of CaO, CuO, and ZnO nanoparticles observed in this study. The results of this study show that callus formation decreased in the stages with decreased POX, and these decreases were seen to have changed depending on the genotypes, type, and period of the nanoparticles applied. This decrease was detected to be changeable depending on the applied NPs. The maximum POX activity was recorded in the presence of NaCl, while its minimum activity was recorded at the 0.8 ppm CuO callus formation stage (Figure 9). Based on our findings, decreases in POX activity in NP-treated callus could be linked to the promotion of callus development parameters and the protective role of NP as direct or indirect. Additionally, induction in POX activity can be explained by the fact that Cu^{+2} ions led to higher ROS generation and initially promoted their antioxidant system to challenge the ROS but then lost the capacity to regulate antioxidant enzyme activity. This is consistent with the earlier report indicating that POX activity is greatly linked to NP ions [52,53]. In the 1st week, Muş applications exhibited enough POX activity mainly due to the rapid and efficient inducer of CuO NPs; however, ZnO was slow and not very effective, which could probably be an outcome of the stronger stability of ZnO. The stability and dissolution characteristics of nanoparticles, as emphasized in Al-Khayri et al. (2023) [48], highlight their implications in plant physiology and uptake behavior. For instance, stability is the main strategy determining the transformation, transport, fate, and toxicity of ZnO NPs in various growth media. This can be explained that the behavior of NPs depends on the intrinsic physiochemical properties and the chemistry of the surrounding different environment media. The nanoparticle uptake mechanisms can be influenced by several factors including salinity, total organic carbon, pH, redox potential, water properties like ionic strength, natural organic material (NOM), redox potential, and other chemical components that influence the short- and long-term behavior of CuO NPs [54,55].

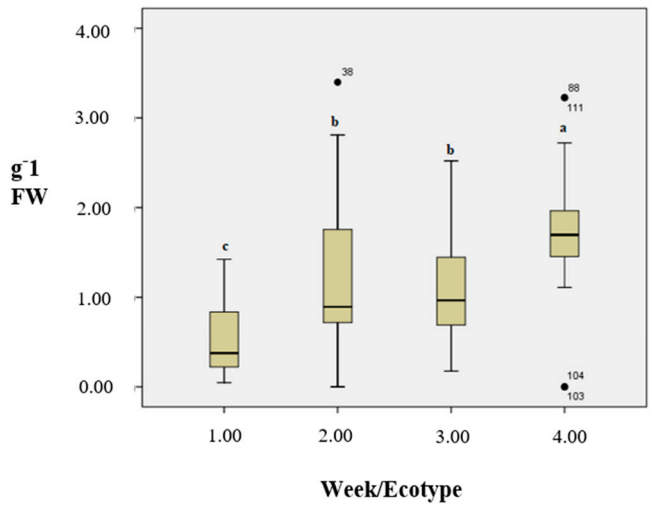


Figure 9. Changes in POX activity *alfalfa* genotypes: 1: First week Muş, 2: First week Erzurum, 3: Second week Muş, 4: Second week Erzurum 1: First week Muş, 2: First Erzurum, 3: Second week Muş, 4: Second week Erzurum. ^{a,b,c} Values with different superscript letters in the same column indicate significant differences ($p \leq 0.05$).

The applied long-term cultured callus cells with 0.8 ppm NPs exhibited the best response and considerably recovered ZnO NPs compared to the control callus in terms of protein content. After NaCl exposure, ZnO showed limited effectiveness in recovering callus at both the induction and formation stages under NaCl stress in comparison to the control and 50 mM NaCl treatments. This explains that ZnO uptake, translocation, and accumulation of ZnO-NPs by plants depend on the distinct features of the NPs and the physiology of the host plant. This can be attributed to the fact that the effects of ZnO on callus cells may be dependent on the concentration and strong systemic activity of the Zn^{+2} ions. These results were similar to an earlier report on expression in response to ZnO uptake [56]. The uptake and biotransformation of ZnO NPs in plants are not only related to concentrations but also particle adhesion onto the cell surface; therefore, ZnO uptake may also arise due to particle dissolution in the culture medium. This suggests that the callus cells were only slightly affected by NaCl severity when 0.8 ppm ZnO was applied. As explained above, CuO was more effective than ZnO on callus cells in response to NaCl severity. It is well known that callus cells within explant resources demonstrate intensive cell division and hence it is necessary for the active synthesis of nucleic acids. The need for DNA production improves the synthesis of NTP, which is an early substrate for nucleic acid synthesis. Increased NTP synthesis increases pH levels within cells. This statement confirms that protein synthesis is significant for plant growth and development, which are highly sensitive to NaCl stress. This observation aligns with molecular evidence provided by Shoukat et al. (2024) [45], who demonstrated upregulated protein synthesis in response to nano-induced abiotic stress. The result may have been verified by the microscopy studies with an SEM, which displays a reduction in the formation of continuous surfaces in the presence of ZnO NPs. In fact, by extending the period of ZnO exposure, the formation of membranous structures, some wrinkles, and amorphous compounds were detected. These effects are likely due to the synthesis of protein and the induction of structural changes in proteins, thus leading to the formation of various conformational changes in the callus surfaces.

5. Conclusions

This study demonstrates that NaCl stress significantly alters the physiological responses of *alfalfa* callus tissues, with the uptake and impact of CuO, ZnO, and CaO NPs playing a central role in mediating these responses. Each NP type exhibited distinct effects on callus tissues, elucidating their potential in mitigating NaCl-induced stress. CuO NPs were the most effective in enhancing salt tolerance, as they reduced H_2O_2 accumulation and supported callus development under prolonged NaCl exposure by modulating ROS levels and decreasing POX activity. ZnO NPs showed more gradual but consistent benefits, likely due to the release of Zn^{2+} ions over time, which promoted protein synthesis and supported callus adaptation, particularly in lower concentrations. In contrast, CaO NPs did not significantly impact antioxidant enzyme activities under NaCl stress but influenced the extracellular matrix by forming mucilage-like structures, contributing to cell wall stabilization and overall structural resilience. Although the mechanisms varied among the NPs, all three nanoparticles effectively reduced MDA levels, balanced H_2O_2 production, and improved protein accumulation, indicating their potential for alleviating NaCl-induced stress. Among them, CuO was the most rapid and effective, followed by ZnO, while CaO mainly focused on structural support. These findings suggest that CuO, ZnO, and CaO NPs hold the potential for improving salt stress tolerance and can be applied to other plant species to tackle various abiotic stresses. Future research should aim to explore the molecular mechanisms of these effects and refine NP application protocols to optimize their use in stress mitigation.

Author Contributions: Conceptualization, M.A.; data curation, B.Y. and H.N.; formal analysis, B.Y., F.B. and H.N.; funding acquisition, M.A.; investigation, M.S.G. and İ.B.; methodology, M.A., M.S.G. and F.B.; project administration, M.S.G.; resource, M.A. and İ.B.; software, F.B.; supervision, B.Y. and İ.B.; validation, M.S.G., B.Y. and O.A.; visualization, M.S.G., F.B. and O.A.; writing—original draft, M.A., H.N. and O.A.; writing—review and editing, M.A., H.N., O.A. and İ.B. All authors have read and agreed to the published version of the manuscript.

Funding: This research received no external funding.

Data Availability Statement: Data are contained within the article.

Conflicts of Interest: The authors have declared that no conflict of interest exists.

References

1. Jalili, F.; Khavazi, K.; Pazira, E.; Nejati, A.; Rahmani, H.A.; Sadaghiani, H.R. Isolation and characterization of ACC deaminase-producing fluorescent Pseudomonads, to alleviate salinity stress on canola (*Brassica napus* L.) growth. *J. Plant Physiol.* **2009**, *166*, 667–674. [CrossRef]
2. Zhu, T.; Deng, X.; Zhou, X.; Zhu, L.; Zou, L.; Li, P.; Zhang, D.; Lin, H. Ethylene and hydrogen peroxide are involved in brassinosteroid-induced salt tolerance in tomato. *Sci. Rep.* **2016**, *6*, 35392. [CrossRef]
3. Jalili, B.; Bagheri, B.; Azadi, S.; Soltani, J. Identification and salt tolerance evaluation of endophyte fungi isolates from halophyte plants. *Int. J. Environ. Sci. Technol.* **2019**, *17*, 3459–3466. [CrossRef]
4. Parida, A.K.; Das, A.B. Salt tolerance and salinity effects on plants. *Ecotoxicol. Environ. Saf.* **2005**, *60*, 324–349. [CrossRef]
5. Parihar, P.; Singh, S.; Singh, R.; Singh, V.P.; Prasad, S.M. Effect of salinity stress on plants and its tolerance strategies: A review. *Environ. Sci. Pollut. Res.* **2015**, *22*, 4056–4075. [CrossRef]
6. Bezirganoglu, I. Response of five triticale genotypes to salt stress in in vitro culture. *Turk. J. Agric. For.* **2017**, *41*, 372–380. [CrossRef]
7. Gao, S.; Yang, L.; Zeng, H.Q.; Zhou, Z.S.; Yang, Z.M.; Li, H.; Zhang, B. A cotton miRNA is involved in regulation of plant response to salt stress. *Int. J. Sci. Rep.* **2016**, *6*, 19736. [CrossRef]
8. Dimpka, C.O.; McLean, J.E.; Latta, D.E.; Manangón, E.; Britt, D.W.; Johnson, W.P.; Maxim, I.B.; Anderson, A.J. CuO and ZnO nanoparticles: Phytotoxicity, metal speciation, and induction of oxidative stress in sand-grown wheat. *J. Nanopart. Res.* **2012**, *14*, 1125. [CrossRef]

9. Castillo-González, J.; Ojeda-Barrios, D.; Hernández-Rodríguez, A.; González-Franco, A.C.; Robles-Hernández, L.; López-Ochoa, G.R. Zinc metalloenzymes in plants. *Interciencia* **2018**, *43*, 242–248.
10. Lian, M.; Wang, J.; Sun, L.; Xu, Z.; Tang, J.; Yan, J.; Zeng, X. Profiles and potential health risks of heavy metals in soil and crops from the watershed of Xi River in Northeast China. *Ecotoxicol. Environ. Saf.* **2019**, *169*, 442–448. [CrossRef] [PubMed]
11. Thor, K. Calcium-nutrient and messenger. *Front. Plant Sci.* **2019**, *10*, 440. [CrossRef]
12. Abeed, A.H.; Al-Huqail, A.A.; Albalawi, S.; Alghamdi, S.A.; Ali, B.; Alghanem, S.M.; El-Mahdy, M.T. Calcium nanoparticles mitigate severe salt stress in *Solanum lycopersicon* by instigating the antioxidant defense system and renovating the protein profile. *S. Afr. J. Bot.* **2023**, *161*, 36–52. [CrossRef]
13. Mahawar, L.; Živčák, M.; Barboricova, M.; Kovár, M.; Filaček, A.; Ferencova, J.; Brestič, M. Effect of copper oxide and zinc oxide nanoparticles on photosynthesis and physiology of *Raphanus sativus* L. under salinity stress. *Plant Physiol. Biochem.* **2024**, *206*, 108281. [CrossRef] [PubMed]
14. Vijayakumar, P.S.; Abhilash, O.U.; Khan, B.M.; Prasad, B.L. Nanogold-Loaded Sharp-Edged Carbon Bullets as Plant-Gene Carriers. *Adv. Funct.* **2010**, *20*, 2416–2423. [CrossRef]
15. Kim, D.H.; Gopal, J.; Sivanesan, I. Nanomaterials in plant tissue culture: The disclosed and undisclosed. *RSC Adv.* **2017**, *7*, 36492–36505. [CrossRef]
16. Iqbal, M.S.; Singh, A.K.; Singh, S.P.; Ansari, M.I. Nanoparticles and plant interaction with respect to stress response. *Nanomater. Environ. Biotechnol.* **2020**, 1–15. [CrossRef]
17. Gohari, G.; Mohammadi, A.; Akbari, A.; Panahirad, S.; Dadpour, M.R.; Fotopoulos, V.; Kimura, S. Titanium dioxide nanoparticles (TiO_2 NPs) promote growth and ameliorate salinity stress effects on essential oil profile and biochemical attributes of Dracocephalum moldavica. *Sci. Rep.* **2020**, *10*, 912. [CrossRef] [PubMed]
18. Ruttkay-Nedecky, B.; Krystofova, O.; Nejdl, L.; Adam, V. Nanoparticles based on essential metals and their phytotoxicity. *J. Nanobiotechnol.* **2017**, *15*, 33. [CrossRef]
19. Wang, P.; Lombi, E.; Zhao, F.J.; Kopittke, P.M. Nanotechnology: A new opportunity in plant sciences. *Trends Plant Sci.* **2016**, *21*, 699–712. [CrossRef] [PubMed]
20. Alabdallah, N.M.; Alzahrani, H.S. The potential mitigation effect of ZnO nanoparticles on [*Abelmoschus esculentus* L. Moench] metabolism under salt stress conditions. *Saudi J. Biol. Sci.* **2020**, *27*, 3132–3137. [CrossRef]
21. Vijai Anand, K.; Reshma, M.; Kannan, M.; Muthamil Selvan, S.; Chaturvedi, S.; Shalan, A.E.; Govindaraju, K. Preparation and characterization of calcium oxide nanoparticles from marine molluscan shell waste as nutrient source for plant growth. *J. Nanostruct. Chem.* **2021**, *11*, 409–422. [CrossRef]
22. Yazıcılar, B.; Böke, F.; Alaylı, A.; Nadaroglu, H.; Gedikli, S.; Bezirganoglu, I. In vitro effects of CaO nanoparticles on Triticale callus exposed to short and long-term salt stress. *Plant Cell Rep.* **2021**, *40*, 29–42. [CrossRef] [PubMed]
23. Prasad, A.; Sidhic, J.; Sarbadhikary, P.; Narayanankutty, A.; George, S.; George, B.P.; Abrahamse, H. Role of metal nanoparticles in organogenesis, secondary metabolite production and genetic transformation of plants under in vitro condition: A comprehensive review. *Plant Cell Tissue Organ Cult.* **2024**, *158*, 33. [CrossRef]
24. Yazıcılar, B.; Bezirganoglu, I. Characterization of the SOS1, SERK1, and WEE1 Conferring a Defense Response to Salt Stress in alfalfa (*Medicago sativa* L.) Callus. *J. Plant Growth Regul.* **2023**, *42*, 7257–7265. [CrossRef]
25. Latif, A.; Sun, Y.; Noman, A. Herbaceous Alfalfa plant as a multipurpose crop and predominant forage species in Pakistan. *Front. Sustain. Food Syst.* **2023**, *7*, 1126151. [CrossRef]
26. Sakiroglu, M.; Brummer, E.C. Identification of loci controlling forage yield and nutritive value in diploid alfalfa using GBS-GWAS. *Theor. Appl. Genet.* **2017**, *130*, 261–268. [CrossRef] [PubMed]
27. Basak, S.; Parajulee, D.; Dhir, S.; Sangra, A.; Dhir, S.K. Improved Protocol for Efficient Agrobacterium-mediated Transformation in *Medicago sativa* L. *Plants* **2024**, *13*, 2992. [CrossRef] [PubMed]
28. Nadaroglu, H.; Alaylı Güngör, A.; Ince, S. Synthesis of nanoparticles by green synthesis method. *Int. J. Innov. Res. Rev.* **2017**, *1*, 6–9.
29. Heath, R.L.; Packer, L. Photoperoxidation in isolated chloroplasts: I. Kinetics and stoichiometry of fatty acid peroxidation. *Arch. Biochem. Biophys.* **1968**, *125*, 189–198. [CrossRef]
30. Jaleel, C.A.; Sankar, B.; Sridharan, R.; Panneerselvam, R. Soil salinity alters growth, chlorophyll content, and secondary metabolite accumulation in Catharanthus roseus. *Turk. J. Biol.* **2007**, *32*, 79–83.
31. Velikova, V.; Yordanov, I.; Edreva, A. Oxidative stress and some antioxidant systems in acid rain-treated bean plants protective role of exogenous polyamines. *Plant Sci.* **2000**, *151*, 59–66. [CrossRef]
32. Yee, Y.; Tam, N.F.Y.; Wong, Y.S.; Lu, C.Y. Growth and physiological responses of two mangrove species (Bruguiera gymnorrhiza and Kandelia candel) to water logging. *Environ. Exp. Bot.* **2003**, *49*, 209–221. [CrossRef]
33. Rolls, G.O.; Farmer, N.J.; Hall, J.B. *Artefacts in Histological and Cytological Preparations*; Leica Biosystems Pty Ltd.: Melbourne, Australia, 2012; p. 106.
34. Minta, A.; Kao, J.P.; Tsien, R.Y. Fluorescent indicators for cytosolic calcium based on rhodamine and fluorescein chromophores. *Biol. Chem.* **1989**, *15*, 8171–8178. [CrossRef]

35. Anantharaman, A.; George, M. Green Synthesis of Calcium Oxide Nanoparticles and Its Applications. *Int. J. Eng. Res. Appl.* **2016**, *6*, 27–31.
36. Meshkatalsadat, M.H.; Zahedifar, M.; Pouramiri, B. Facile Green Synthesis of CaO NPs Using the Crataegus Pontica C.Koch Extract for Photo-Degradation of MB Dye. *Environ. Sci. Pollut. Res.* **2022**, *29*, 54688–54697. [CrossRef]
37. Sahu, G.; Saha, S.; Datta, S.; Chavan, P.; Naik, S. Methanolysis of Jatropha curcas oil using K_2CO_3/CaO as a solid base catalyst. *Turk. J. Chem.* **2017**, *41*, 845–861. [CrossRef]
38. Nadaroglu, H.; Alaylı Gungor, A. Highly sensitive glucose sensor based on ZnO NPs as a biomimetic enzyme. *Biosci. Res.* **2020**, *17*, 775–785.
39. Gultekin, D.D.; Alaylı, A.; Nadaroglu, H. Eco-friendly synthesis of nano copper and its use in Fenton-like reactions for methylene blue degradation. *Int. J. Chem. Tech.* **2020**, *4*, 71–78. [CrossRef]
40. Grodetskaya, T.A.; Evlakov, P.M.; Fedorova, O.A.; Mikhin, V.I.; Zakharova, O.V.; Kolesnikov, E.A.; Gusev, A.A. Influence of copper oxide nanoparticles on gene expression of birch clones in vitro under stress caused by phytopathogens. *Nanomaterials* **2022**, *12*, 864. [CrossRef]
41. Gunasena, M.D.K.M.; Alahakoon, A.M.P.D.; Polwaththa, K.P.G.D.M.; Galpaya, G.D.C.P.; Priyanjani, H.A.S.A.; Koswattage, K.R.; Senarath, W.T.P.S.K. Transforming Plant Tissue Culture with Nanoparticles: A Review of Current Applications. *Plant Nano Biol.* **2024**, *10*, 100102. [CrossRef]
42. Singh, Y.; Kumar, U.; Panigrahi, S.; Balyan, P.; Mehla, S.; Sihag, P.; Dhankher, O.P. Nanoparticles as novel elicitors in plant tissue culture applications: Current status and future outlook. *Plant Physiol. Biochem.* **2023**, *203*, 108004. [CrossRef] [PubMed]
43. Wang, Z.; Li, H.; Li, X.; Xin, C.; Li, S.; Li, Y.; Zheng, X.; Li, H.; Wei, X.; Zhang, Z.; et al. Naomo-ZnO priming induces salt tolerance by promoting photosynthetic carbon assimilation in wheat. *Arch. Agron. Soil. Sci.* **2019**, *66*, 1259–1273. [CrossRef]
44. Javed, R.; Usman, M.; Yücesan, B.; Zia, M.; Gürel, E. Effect of zinc oxide (ZnO) nanoparticles on physiology and steviol glycosides production in micro propagated shoots of Stevia rebaudiana Bertoni. *Plant Physiol. Biochem.* **2017**, *110*, 94–99. [CrossRef] [PubMed]
45. Shoukat, A.; Pitann, B.; Zafar, M.M.; Farooq, M.A.; Haroon, M.; Nawaz, A.; Saqib, Z.A. Nanotechnology for climate change mitigation: Enhancing plant resilience under stress environments. *J. Plant Nutr. Soil. Sci.* **2024**, *187*, 604–620. [CrossRef]
46. Ditta, A.; Arshad, M. Applications and perspectives of using nanomaterials for sustainable plant nutrition. *Nanotechnol. Rev.* **2016**, *5*, 209–229. [CrossRef]
47. Liu, R.H.; Kang, Y.H.; Pei, L.; Wan, S.Q.; Liu, S.P.; Liu, S.H. Use of a new controlled-loss-fertilizer to reduce nitrogen losses during winter wheat cultivation in the Danjiangkou Reservoir Area of China. Commun. *Soil. Sci. Plant. Anal.* **2016**, *47*, 1137–1147. [CrossRef]
48. Al-Khayri, J.M.; Rashmi, R.; Surya Ulhas, R.; Sudheer, W.N.; Banadka, A.; Nagella, P.; Almaghasla, M.I. The role of nanoparticles in response of plants to abiotic stress at physiological, biochemical, and molecular levels. *Plants* **2023**, *12*, 292. [CrossRef]
49. Zari, H.; Babak, P.; Asad, R. The Effect of Priming with Nano-sliver on Agronomic Traits of Safflower Cultivars. *J. Essent. Oil-Bear. Plants* **2015**, *18*, 1148–1156. [CrossRef]
50. Aazami, M.A.; Rasouli, F.; Ebrahimzadeh, A. Oxidative damage, antioxidant mechanism, and gene expression in tomato responding to salinity stress under in vitro conditions and application of iron and zinc oxide nanoparticles on callus induction and plant regeneration. *BMC Plant Biol.* **2021**, *21*, 597. [CrossRef]
51. Soleymanzadeh, R.; Iranbakhsh, A.; Habıbı, G.; Ardebılı, Z.O. Selenıum nanopartıcle protected strawberry against salt stress through modifications in salicylic acid, ion homeostasis, antioxidant machinery, and photosynthesis performance. *Acta Biol. Crac. Ser. Bot.* **2020**, *62*, 33–42. [CrossRef]
52. Liang, W.; Ma, X.; Wan, P.; Liu, L. Plant salt-tolerance mechanism: A review. *Biochem. Biophys. Res. Commun.* **2018**, *495*, 286–291. [CrossRef]
53. Jadczak, P.; Kulpa, D.; Drozd, R.; Przewodowski, W.; Przewodowska, A. Effect of AuNPs and AgNPs on the antioxidant system and antioxidant activity of lavender (*Lavandula angustifolia* Mill.) from in vitro cultures. *Molecules* **2020**, *25*, 5511. [CrossRef]
54. Sousa, V.S.; Teixeira, M.R. Aggregation kinetics and surface charge of CuO nanoparticles: The influence of pH, ionic strength and humic acids. *Environ. Chem.* **2013**, *10*, 313–322. [CrossRef]
55. Conway, J.R.; Adeleye, A.S.; Gardea-Torresdey, J.; Keller, A.A. Aggregation, Dissolution, and Transformation of Copper Nanoparticles in Natural Waters. *Environ. Sci. Technol.* **2015**, *49*, 2749–2756. [CrossRef] [PubMed]
56. da Cruz, T.N.; Savassa, S.M.; Montanha, G.S.; Ishida, J.K.; de Almeida, E.; Tsai, S.M.; Pereira de Carvalho, H.W. A new glance on root-to-shoot in vivo zinc transport and time-dependent physiological effects of $ZnSO_4$ and ZnO nanoparticles on plants. *Sci. Rep.* **2019**, *9*, 10416. [CrossRef]

Disclaimer/Publisher's Note: The statements, opinions and data contained in all publications are solely those of the individual author(s) and contributor(s) and not of MDPI and/or the editor(s). MDPI and/or the editor(s) disclaim responsibility for any injury to people or property resulting from any ideas, methods, instructions or products referred to in the content.